# Effects of temperature and pressure on phonons in FeSi_{1−x}Al_{x}

O. Delaire, I. I. Al-Qasir, J. Ma, A. M. dos Santos, B. C. Sales, L. Mauger, M. B. Stone, D. L. Abernathy, Y. Xiao, and M. Somayazulu

Phys. Rev. B **87**, 184304 — Published 31 May 2013

DOI: 10.1103/PhysRevB.87.184304

# Effects of temperature and pressure on phonons in $FeSi_{1-x}Al_x$.

O. Delaire[1], I. I. Al-Qasir[1], J. Ma[1], A. M. dos Santos[1], B. C. Sales[1],
L. Mauger[2], M. B. Stone[1], D. L. Abernathy[1], Y. Xiao[3], and M. Somayazulu[4]
*1. Oak Ridge National Laboratory, 1, Bethel Valley road,
Oak Ridge, TN 37831, USA 2. California Institute of Technology,
W. M. Keck Laboratory 138-78, Pasadena, CA 91125, USA 3. HPCAT,
Geophysical Laboratory, Carnegie Institution of Washington,
Argonne, IL 60439, USA 4. Geophysical Laboratory,
Carnegie Institution for Science, Washington, D.C., 20015, USA*
(Dated: May 1, 2013)

The effects of temperature and pressure on phonons in B20 compounds $FeSi_{1-x}Al_x$ were measured using inelastic neutron scattering (INS) and nuclear-resonant inelastic x-ray scattering (NRIXS). The effect of hole-doping through Al substitution is compared to results of alloying with Co (electron-doping) in $Fe_{1-x}Co_xSi$. While the temperature dependence of phonons in FeSi is highly anomalous, doping with either type of carriers leads to a recovery of the normal quasi-harmonic behavior. Density functional theory (DFT) computations of the electronic band structure and phonons were performed. The anomaly in the temperature-dependence of the phonons in un-doped FeSi was related to the narrow band gap, and its sensitivity to the effect of thermal disordering by phonons. On the other hand, the pressure dependence of phonons at room temperature in un-doped FeSi follows the quasi-harmonic behavior, and is well reproduced by the DFT calculations.

PACS numbers:

## I. INTRODUCTION

FeSi is a peculiar material, and has generated interest for decades. At low pressures and temperatures, the stable structure of FeSi is the B20 cubic phase[1], but under high pressure and high temperature it transforms to the simpler B2 phase (CsCl-type)[2]. The B20 phase has rather low symmetry ($T^4\,P2_13$), which can be derived from the rocksalt arrangement by a distortion of Fe-Si nearest-neighbor pairs along $\langle 111\rangle$ directions, yielding seven-fold coordination at the Fe and Si sites[1]. FeSi has generated great interest as a possible $d-$electron Kondo insulator[3–6], as well as a possible product from the reaction between molten iron and mantle silicates at the core-mantle boundary[2,7–9]. Many physical properties of FeSi display anomalous temperature dependences, which has been related to its peculiar electronic band structure[10–16,18]. For example, the magnetic susceptibility, heat capacity, thermal expansion, and elastic properties all show anomalous temperature dependences between 0 K and 800 K[15–17]. These anomalies have been related to the effect of thermal disorder (disruption from ideal atomic lattice owing to atomic vibrations at finite temperature) on the narrow band-gap[19–24], as well as possible electronic correlation effects[3,25].

Photoemission measurements on FeSi have been initially interpreted in terms of strong electronic correlations and a possible Kondo scenario[3,6,10]. However, recent angle-resolved photoemission measurements indicate that the electronic structure can be described in terms of an itinerant model, and show no Kondo peak[4,5,26]. In addition, strong-correlation effects have been inferred from optical measurements[27], although this point is somewhat debated[29]. Recent studies have also highlighted the importance of electron-phonon coupling[23,24,27,30,31]. Importantly, the electronic band structure may show a strong sensitivity to thermal disorder, owing to the narrowness of the gap[19–24]. Early phenomenological models of FeSi have considered thermal carrier excitations between two thin bands across a narrow gap of width, $E_g \sim 80$ meV[12,15,16]. Density functional theory (DFT) calculations of the electronic density of states (DOS) of B20 FeSi at 0 K have indeed found a narrow gap $E_g \sim 100$ meV with sharp peaks on either side[13,14,18,19,23]. However, most descriptions have not considered the effect of atomic motions necessarily present at $T > 0$ K, except[19–23].

The renormalization of a material's electronic structure by thermal disorder can be significant at high temperature, which is of relevance for thermoelectric applications, for example[23,32]. Temperature-dependent photo-emission and ellipsometry measurements[4,27,28] have shown that the narrow gap is strongly dependent on temperature, and closes around room temperature. Systems with sharp structures in their electronic density of states (DOS) near the Fermi level can be particularly sensitive to thermal excitation of phonons, as well as alloying effects[33–35]. This leads to adiabatic electron-phonon coupling effects which are important in the context of thermoelectric properties[35–37], and which can influence the thermodynamics of the system[38].

The thermal atomic motions (phonons) in FeSi cause a strong renormalization of the electronic structure, filling the gap[19,23], which in turn leads to anomalies in the temperature dependence of phonons[23]. The metallization of FeSi with increasing $T$ provides a large number of carriers at the Fermi level, which efficiently screen the interatomic force-constants, leading to an anomalously strong softening. CoSi, which is isostructural but metallic at all tem-

peratures, is not affected by this renormalization because its Fermi level is located in a region of the electronic DOS that is not sensitive to the thermal disordering, and its Fermi level electronic density, $N(E_F)$, is rather constant with temperature. Calculations of electronic correlation effects with dynamical mean-field theory (DMFT) have also predicted a filling of the narrow gap with incoherent spectral weight upon increasing temperature[25], and it is possible that both effects are simultaneously at play. We note, however, that in the DMFT calculation of Tomczak *et al.*[25], the filling of the gap with increasing $T$ occurs significantly slower than observed experimentally[4,28]. Thus, it would be interesting for DMFT calculations to incorporate thermal atomic displacements, which necessarily occur at finite temperatures.

The strong electron-phonon coupling has clearly been observed in transport measurements of electron-doped FeSi[24]. Here we compare the effects of hole- and electron-doping on the phonons, by substituting Al on the Si site or Co on the Fe site, respectively. Full solubility is achieved on the Fe sublattice in the $Fe_{1-x}Co_xSi$ pseudo-binary alloys, and the system goes from semiconductor ($x = 0$) to a complex magnetic metal (for $0.1 < x < 0.8$), and finally a diamagnetic semimetal ($x = 1.0$), with increasing Co concentration[39,40]. Interestingly, $Fe_{1-x}Co_xSi$ ($0.1 < x < 0.8$) has been reported to form complex helical spin textures, including a skyrmion lattice in $Fe_{0.5}Co_{0.5}Si$[41]. The Al-doped phase $FeSi_{1-x}Al_x$ also forms the B20 structure, for concentrations $x_{Al} \lesssim 0.2$. Doping with Al leads to a fast increase in electrical conductivity, and the Al-doped FeSi has been reported to be an unusual heavy-fermion metal[6,10]. It is therefore interesting to compare the effects of hole and electron doping on the phonons.

We report inelastic neutron scattering (INS) and nuclear-resonant inelastic x-ray scattering (NRIXS) measurements of the phonon density of states (DOS) of $FeSi_{1-x}Al_x$, for $x = 0.0, 0.03, 0.1$, as well as first-principles calculations of the phonons and electronic-structure. The phonon DOS of $FeSi_{1-x}Al_x$ was measured as a function of temperature with INS ($5 \leqslant T \leqslant 700\,\mathrm{K}$), and the Fe-partial phonon DOS was measured as a function of pressure with NRIXS ($0 \leqslant P \leqslant 18\,\mathrm{GPa}$).

## II. SAMPLE PREPARATION

Polycrystalline ingots of FeSi and $FeSi_{0.9}Al_{0.1}$ were prepared by arc-melting pieces of the respective elements (better than 99.99% purity) in appropriate proportions, under an ultra-pure Ar atmosphere. For NRIXS studies, FeSi and $FeSi_{0.95}Al_{0.05}$ samples were prepared with 95% enrichment in $^{57}$Fe. No oxidation was detected on the ingots after melting. The mass loss upon arc-melting was negligible. The resulting ingots were pulverized, and examined with x-ray diffraction. The x-ray diffraction patterns for all samples were consistent with the B20 structure. No secondary phases were observed.

## III. INELASTIC NEUTRON SCATTERING

Inelastic neutron scattering (INS) spectra were measured using the ARCS time-of-flight chopper spectrometer at the Spallation Neutron Source[42], at Oak Ridge National Laboratory. Measurements were performed at low temperatures with a closed-cycle He refrigerator, and at high temperatures using a low-background resistive furnace. The measurements were performed with the samples encased in a thin-walled Al can, filled with a low pressure of helium. We used incident neutron energies $E_i = 80\,\mathrm{meV}$ and $100\,\mathrm{meV}$. The energy resolution (full width at half max.) with $E_i = 100\,\mathrm{meV}$ was about 1.5 meV at 60 meV neutron energy loss, increasing to about 4 meV at the elastic line (better at $E_i = 80\,\mathrm{meV}$). The empty Al sample container was measured in identical conditions at all temperatures.

The data were normalized by the total incident flux, corrected for detector efficiency, and mapped from instrument coordinates to the physical momentum-transfer, $Q$, and energy-transfer, $E$, using the MANTID reduction software[43]. The scattering from the empty container was analyzed in the same conditions, and subtracted from the data. The analysis of the phonon DOS was performed in the incoherent scattering approximation, which is reliable in the case of powders and large integration volumes in reciprocal space ($Q \lesssim 10\,\mathring{A}^{-1}$). The elastic peak was subtracted, and the data for $E < 6\,\mathrm{meV}$ were extrapolated with a Debye-like quadratic energy dependence. A standard procedure was used to correct for the effect of multiphonon scattering[44].

For a monatomic crystal of cubic symmetry, this analysis provides the phonon DOS. However, in a non-monatomic crystal, different elements have different ratios of cross-section over mass, $\sigma/M$, and the vibration modes corresponding to motions of elements with larger $\sigma/M$ are over-emphasized, resulting in a generalized phonon DOS. The values of $\sigma/M$ for (Fe, Co, Si, Al) are (0.208, 0.095, 0.077, 0.056) b/amu, respectively. Thus, the modes involving large motions of Fe atoms are overemphasized in the measured phonon DOS. However, the change in neutron-weights between $FeSi_{0.9}Al_{0.1}$ and FeSi is not a concern, enabling a straightforward comparison for Al-alloying effects. Also, the neutron-weighting does not affect significantly the $T$-dependence observed in our measurement. We performed a correction for neutron-weighting for data at 300 K and ambient pressure, using the partial phonon DOS for Fe atoms measured with NRIXS. By comparing the neutron-weighted and de-weighted phonon spectra, we find that the effect of neutron-weighting leads to a 7% underestimate of the average phonon energy, $\langle E \rangle$, and the Debye temperature, $\theta_D$, in the raw INS data.

The neutron-weighted phonon DOS curves are shown in Fig. 1. The bottom panel shows a softening of the phonon DOS between FeSi and $FeSi_{0.9}Al_{0.1}$ at 5 K. This softening is fairly large ($-3.7\%$), and results from a combination of lattice parameter increase, and of the intro-

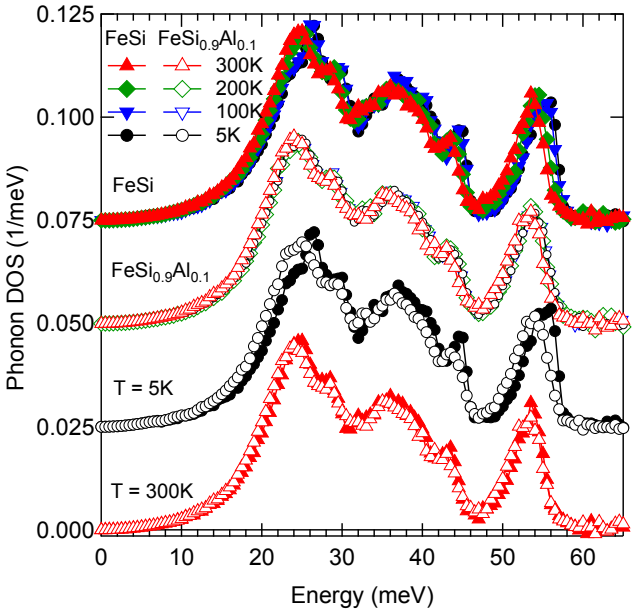


FIG. 1: Phonon DOS of FeSi (full symbols) and $FeSi_{0.9x}Al_{0.1}$ (open symbols), measured with INS at $T = 5, 100, 200, 300$ K ($E_i = 80$ meV). Curves are vertically offset for clarity. The two top sets of curves are for FeSi and $FeSi_{0.9x}Al_{0.1}$ as a function of temperature. The two bottom sets are comparing the phonon DOS of FeSi and $FeSi_{0.9}Al_{0.1}$ at $T = 5$ K and at $T = 300$ K. Statistical error bars are smaller than symbols.

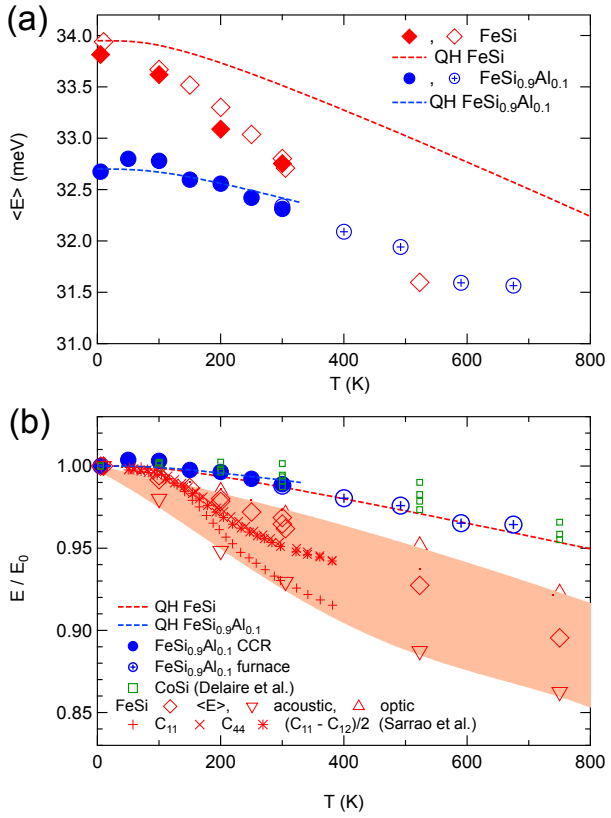


FIG. 2: (a) Average phonon energy (neutron-weighted first-moment of the phonon DOS measured with INS) for FeSi and $FeSi_{0.9}Al_{0.1}$ *vs* temperature. (b) Relative change (compared with lowest $T$) for several phonon energies and elastic constants, as a function of temperature. Experimental error bars are comparable to the size of the symbols. The dashed curves show the expected temperature dependence in the quasiharmonic model (QH), using the thermal Grüneisen parameters from our DFT calculations and experimental thermal expansion (see below). For FeSi, thermal expansion data were taken from[47]. The crosses and stars show the relative change in elastic moduli of FeSi measured by Sarrao *et al.*[45]. Open green circles are data for average phonon energy in CoSi from Delaire *et al.*[23].

duction of free-carriers (holes). Based on our measurements of lattice parameters (see below), alloying with 10% Al leads to an increase of 0.39% in lattice parameter, leading to an expected suppression of $-1.9\%$ in $\langle E \rangle$, taking an average Grüneisen parameter $\gamma = 1.6$ for FeSi, as calculated with DFT (or -2.6% if using the experimental value $\gamma = 2.2$). The volume effect alone thus appears slightly smaller than the observed phonon softening. This difference could reflect the additional effect of the metallization of the system upon Al doping, which increases screening and lowers the interatomic force-constants. That effect is seen clearly in the comparison of the temperature dependence of pure and doped compounds below. The very small mass difference between Al and Si ($\omega \sim M^{-1/2}$) only has a minimal effect, especially for 10% Al substitution.

As can be seen on Fig. 1, the phonon DOS of FeSi and $FeSi_{0.9}Al_{0.1}$ also exhibit very different behaviors as function of temperature. In the case of $FeSi_{0.9}Al_{0.1}$, there is only a small difference in the phonon DOS measured at 5 K and at 300 K, compatible with the limited thermal expansion in this range. On the other hand, the DOS of FeSi softens considerably, with all parts of the spectrum shifting to lower energies. This softening is about 2 meV both for the acoustic peak at 25 meV, and for the Si peak at 55 meV.

In Fig. 2, we plot the temperature dependence of the (neutron-weighted) average phonon energy, obtained as the first-moment of the measured phonon DOS. As can be seen on this figure, phonons soften much more rapidly in FeSi than in $FeSi_{0.9}Al_{0.1}$. This softening is already pronounced between 5 K and 300 K, and affects the full phonon spectrum, as can be seen in Fig. 1. Above 300 K, the phonon energies of FeSi and $FeSi_{0.9}Al_{0.1}$ become more similar. We computed the expected mode softening in the quasiharmonic approximation (QH) using experimental thermal expansion data ([16,47]), and the experimental Grüneisen parameter for FeSi reported in[47]. These QH curves are indicated by dashed lines in Fig. 2. One can see that the amount of softening observed in FeSi phonons is strongly anomalous: it is more than 4 times larger than the QH prediction for acoustic modes at 300 K. On the other hand, phonon energies in $FeSi_{0.9}Al_{0.1}$ are in good agreement with the QH model (within experimen-

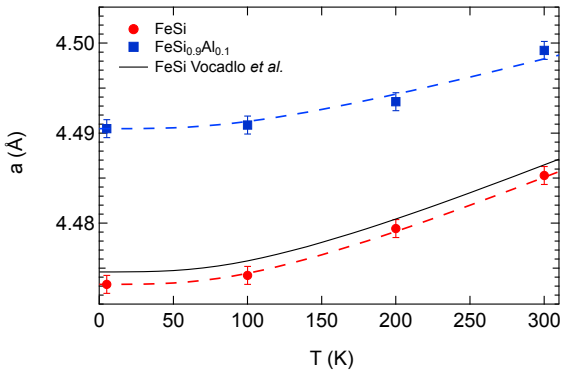


FIG. 3: Lattice parameters of FeSi and $FeSi_{0.9}Al_{0.1}$ obtained from neutron scattering data measured on ARCS. The solid curve is from Ref. 47. Dashed lines are fits of thermal expansion behavior, see text.

tal uncertainty), and very similar to previous results for CoSi[23].

Our observations of anomalously large softening of phonons with increasing temperature in FeSi are compatible with the reported behavior of some elastic constants, particularly $C_{11}$ and the shear elastic constants $C_{44}$ and $(C_{11}-C_{12})/2$, as shown in Fig. 2[45,46]. Our phonon DOS measurements also show that all phonons are affected, which has important thermodynamic consequences.

A Debye temperature can be obtained from the first-moment of the phonon spectrum, as $\theta_D = 4/3\,\langle E\rangle/k_B$, where $\langle E\rangle = \int E\,g(E)dE$[48]. We find: $\theta_D = 530 \pm 10\,K$ using the de-weighted phonon DOS $g(E)$ from INS at 300 K. This value is compatible with the estimate provided by Vočadlo *et al.* based on fits of thermal expansion data from diffraction measurements $(525 \pm 6\,K)$[47]. By considering the partial DOS for Fe vibrations, $g_{Fe}(E)$ measured with NRIXS at 300 K (see below), we obtain $\theta_D^{Fe} = 465 \pm 5\,K$.

The lattice parameters of FeSi and $FeSi_{0.9}Al_{0.1}$ were extracted from the elastic channel of the ARCS data, by fitting 13 diffraction peaks at $1.95 \leqslant Q \leqslant 9.4\,Å^{-1}$, and performing a Nelson-Riley analysis. The results for data at temperatures $5 \leqslant T \leqslant 300\,K$ are plotted in Fig. 3. The results for FeSi are in excellent agreement with the reported measurement of Vočadlo *et al.*[47] (with a systematic shift of $-0.0014$ Å), validating our analysis procedure. As can be seen on this figure, the introduction of Al leads to an increase in lattice parameter (+0.39% at 5 K and +0.31% at 300 K). This is in good agreement with values reported by DiTusa *et* al. (Ref. 11). It is worthy to note that thermal expansion is larger in FeSi than in $FeSi_{0.9}Al_{0.1}$, which is compatible with the larger phonon softening in FeSi than $FeSi_{0.9}Al_{0.1}$. Since we have too few temperature points to extract a thermal expansion coefficient, we make the simple assumption that the thermal expansion coefficient $\alpha_{FeSi_{0.9}Al_{0.1}}(T)$ has the same $T$ dependence as $\alpha_{FeSi}(T)$. Fitting the scaling coefficient, we obtain the dashed lines in Fig. 3, and we estimate a 35% suppression in linear thermal expansion for 10% Al alloying over the range $10 \leqslant T \leqslant 300\,K$. The effect is particularly large for $100 \leqslant T \leqslant 200\,K$, where $\alpha_{.FeSi}/\alpha_{FeSi_{0.9}Al_{0.1}} = 1.2\times10^{-5}\,K^{-1}/5.8\times10^{-6}\,K^{-1} \simeq 2$, in good agreement with the extra softening observed in the phonon energies (cf Fig. 2-a). We note that our estimate for FeSi is in good agreement with $\alpha_{FeSi}(T = 200\,K) = 1.3\times10^{-5}\,K^{-1}$ reported by Krentsis *et al.*[17]

## IV. NUCLEAR-RESONANT INELASTIC X-RAY SCATTERING

Nuclear resonant inelastic x-ray scattering (NRIXS) measurements[49,50] were performed at high pressures at beamline 16-IDD (HP-CAT) at the Advanced Photon Source at the Argonne National Laboratory. In all measurements, the incident photon energy was tuned to 14.4124 keV, the nuclear resonance energy of $^{57}$Fe. The NRIXS signal was measured with multiple avalanche photodiode detectors positioned 90° from the direction of the beam. Data were collected in scans of incident photon energy, with $\Delta E = -80$ to $+80$ meV from the resonant energy, in steps of 0.5 meV. The experimental energy resolution function was measured with a single avalanche photodiode placed in the forward beam direction, recording the intensity as a function of the shift of the incident energy away from the $^{57}$Fe resonance energy (the data for the instrument resolution were summed over all runs performed in the same conditions). The monochromator energy resolution (full width at half maximum) was 2.2 meV.

All of the NRIXS data reduction were performed using the software PHOENIX[50,51]. The raw NRIXS spectra, given as intensity versus the angle of the monochromator crystals, were converted to intensity versus energy transfer. The first few bins on the low energy side were used to determine an energy independent background, which was removed for all energy transfers. The elastic peak was removed using the measured resolution function. The contribution from multiphonon scattering processes was subtracted using a self-consistent procedure based on a Fourier-log method[51], and the Fe-partial phonon density of states was obtained by correcting for the thermal occupation factor.

Measurements as function of pressure were performed in panoramic diamond-anvil cells (DAC), fitted with 500 $\mu$m culet diamonds and a Be gasket drilled with a 130 micron hole. The sample was $\sim 100\,\mu$m-wide. The pressure medium was silicone oil. The pressure inside the DAC was determined through the fluorescence line of ruby crystals loaded with the samples in the pressure medium[52]. Measurements were performed with the cell at ($P$=0, 4, 11, and 18 GPa).

The $^{57}$Fe-partial phonon DOS of FeSi as a function of pressure is shown in Fig. 4. The range of phonon energies at ambient pressure is in excellent agreement with the INS measurements of the total phonon DOS.

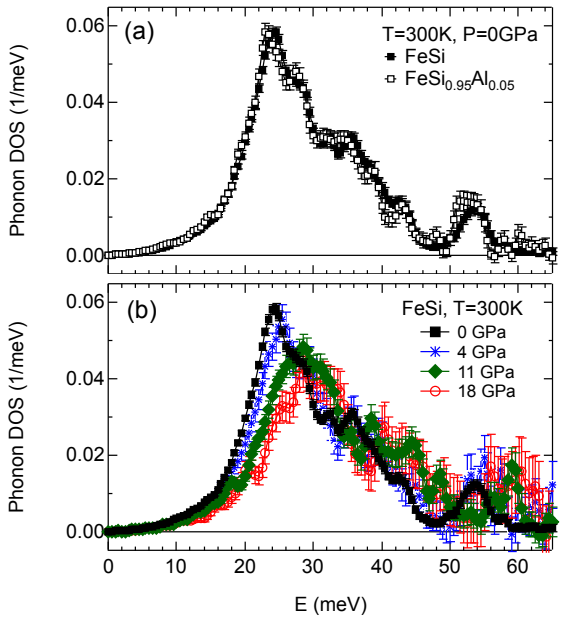


FIG. 4: (a) NRIXS measurement of $^{57}$Fe partial phonon DOS in FeSi and $FeSi_{0.95}Al_{0.05}$ at 300 K, 0 GPa. (b) Fe partial DOS in FeSi at $P = 0, 4, 11, 18$ GPa ($T = 300$ K).

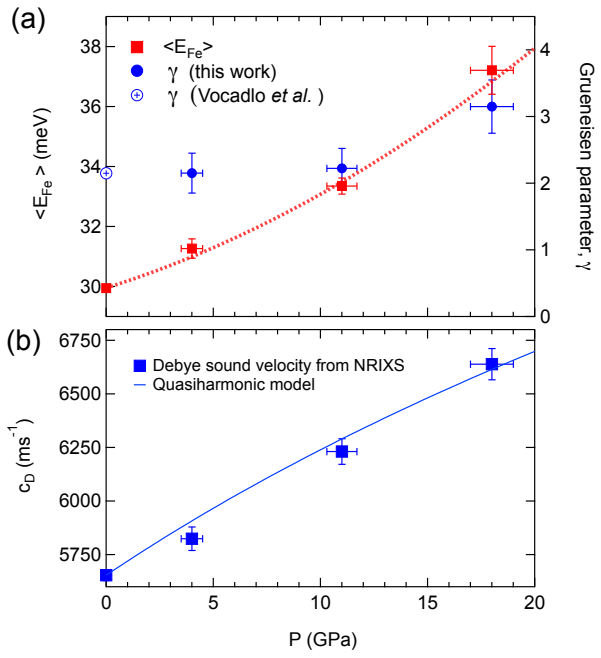


FIG. 5: (a) Average phonon energy for Fe vibrations, determined from NRIXS measurements, as a function of pressure, and corresponding Grüneisen parameter. The Grüneisen parameter at ambient pressure is obtained from Vočadlo *et al.*, Ref 47. The dotted red line is a guide to the eye. (b) Polycrystalline-averaged Debye sound velocity from acoustic portion of the partial DOS measured with NRIXS. The curve shows the expected quasiharmonic behavior based on the equation-of-state reported in Ref. 8.

One may also distinctly recognize the different features of the DOS (peak positions). The NRIXS measurement shows that vibrational amplitudes of Fe atoms have a larger contributions to the phonon polarization vectors for lower vibration frequencies, especially $E \leqslant 35$ meV. The stronger intensity of the Fe-partial DOS at lower energies reflects the mass-ratio of Fe and Si, with the motions of heavier Fe atoms more prominent at low frequencies. This induces a skewing of the INS phonon DOS, in which the Fe modes are over-emphasized, as previously noted. However, the knowledge of the Fe-partial phonon DOS enables a correction for neutron-weighting (see below). Fig. 4-a compares the $^{57}$Fe-partial phonon DOS of FeSi and $FeSi_{0.95}Al_{0.05}$. As may be seen on this figure, 5% Al substitution induces a slight softening of the Fe-phonon DOS, compatible with softening of the total DOS obtained with 10% Al. The effect on the Si partial DOS may be larger, but cannot be measured with this technique.

As shown in Fig. 4-b, with increasing pressure, the Fe-partial phonon DOS systematically shifts toward higher energies, corresponding to a stiffening of interatomic force-constants, owing to compression. From the measured DOS, we extracted the average Fe phonon energy $\langle E_{\rm Fe}\rangle$, *vs* pressure, $P$, shown in Fig. 5-a. From the volume-derivative of $\langle E_{\rm Fe}\rangle$, we obtained the Grüneisen parameter for Fe modes. At lower pressures, we find $\gamma_{\rm Fe} = 2.2 \pm 0.3$, in excellent agreement with the value of thermal Grüneisen parameter, $\gamma_{\rm th} = 2.15$ at 300 K, reported by Vočadlo *et al.*[47].

By fitting the low-energy, acoustic portion ($0 \leqslant E \leqslant 15$ meV) of the NRIXS Fe partial DOS to a Debye behavior, we obtained the following values of Debye sound velocities, $c_{\rm D} = 5654 \pm 26$, $5824 \pm 55$, $6231 \pm 60$, $6639 \pm 73\, ms^{-1}$ at pressures P = 0, 4, 11, 18 GPa, respectively. These are plotted in Fig. 5-b. Using the acoustic portion of the INS data for the FeSi phonon DOS at 300 K, we obtain $c_{\rm D} = 5756 \pm 80\, ms^{-1}$, in good agreement with the NRIXS result. These values are about 10% larger than values derived from shear and compression velocities (polycrystalline averages) calculated with DFT (B20 phase, GGA)[9], using the relation $3/c_{\rm D}^3 = 2/c_S^3 + 1/c_L^3$, which yields: $c_{\rm D} = 5110, 5550, 5830\, ms^{-1}$ at P = 0, 10, 20 GPa, respectively. The stiffening of sound velocities with pressure obtained from NRIXS between 0 and 18 GPa is about 17%, which is in excellent agreement with the equation of state $V(P)$ reported by Lin *et al.* ( $\Delta V/V = -7.75\%$ at 18 GPa) and $\bar{\gamma} = 2.2$, also resulting in 17% stiffening[8]. Thus, the pressure dependence (up to 18 GPa, at 300 K) of phonons and elastic constants follows the expected quasi-harmonic behavior, while their temperature dependence at ambient pressure is anomalous.

## V. FIRST-PRINCIPLES SIMULATIONS

Density Functional Theory (DFT) calculations were conducted with the software VASP, using the projector augmented wave formalism[53–55], and the PBE-96 generalized gradient exchange-correlation functional[56]. A convergence study motivated the use of a $12 \times 12 \times 12$ grid of $k-$points for the 8–atom cell, corresponding to 76 $k-$points in the irreducible portion of the Brillouin zone. Computations of phonons were performed on $2 \times 2 \times 2$ supercells, with a $6 \times 6 \times 6$ $k-$point grid. The energy cutoff in all calculations was 600 eV. The positions of the ions and the unit cell volume were optimized to minimize forces on the nuclei and the overall energy. The optimized lattice parameter were 4.4492 Å for FeSi, 4.4839 Å for $Fe_4Si_3Al_1$, and 4.4526 Å for $Fe_{32}Si_{31}Al_1$. Scaled to 10% Al alloying, these represent increases in lattice parameter of 0.23% and 0.31%, respectively, in good agreement with our measurement (0.39% at 5K). Spin-polarized calculations were conducted on the optimized FeSi structure, and no magnetic ordering was found.

### A. Electronic Structure

The electronic densities of states of FeSi and $Fe_{32}Si_{31}Al_1$ were computed on the optimized structures, using a fine $k-$point mesh and tetrahedron integration. Results are shown in Fig. 6 (the reference of energy is taken as the top of the valence band in the case of FeSi). In $Fe_{32}Si_{31}Al_1$, the introduction of holes leads to a Fermi level shifted into the peak at the top if the valence band. The calculated electronic DOS of FeSi, $Fe_4Si_3Al_1$, and $Fe_{32}Si_{31}Al_1$ are similar, with that of Al-doped cells gradually shifted to higher energies, corresponding to a rigid shift of the DOS with higher Al content. Our calculations predict a gap of about 120 meV in FeSi. This is somewhat larger than measured experimentally[27], and could explain why the effect of electron-phonon coupling on the phonons happens on a larger $T$ scale in calculations than in experiment[23]. For $Fe_{32}Si_{31}Al_1$, the gap is about 160 meV and it is about 100 meV in $Fe_4Si_3Al_1$.

### B. Lattice Dynamics

The phonon DOS and dispersions of FeSi and $Fe_4Si_3Al_1$ were computed form first principles, using the small displacement method (FeSi), and $2 \times 2 \times 2$ supercells (64 atoms). These phonon DOS computations were based on the ideal periodic B20 structure, and thus are not expected to capture the effect of thermal disorder on the underlying band structure and on the phonons. The phonon DOS was computed at the theoretical equilibrium lattice parameter ($a_0 = 4.4492\mathring{A}$ for FeSi) and at the experimental 300 K lattice parameter, with ion positions optimized at each volume. The DOS and dispersions computed at the theoretical lattice parameters are

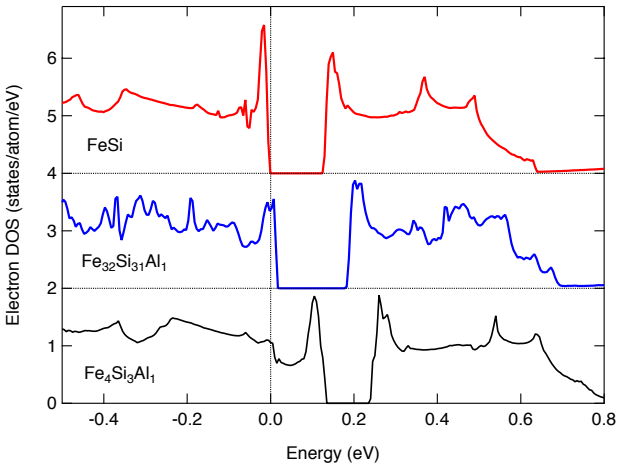


FIG. 6: Electronic DOS of B20 FeSi and $Fe_{32}Si_{31}Al_1$ calculated from first-principles, on relaxed structures at theoretical equilibrium volumes. The curves for FeSi and $Fe_{32}Si_{31}Al_1$ are shifted vertically by 4 and 2 states/atom/eV, respectively.

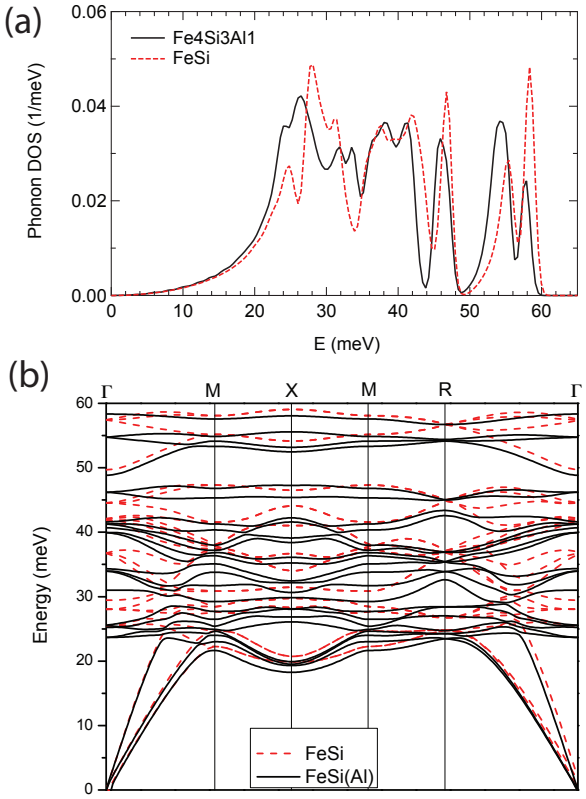


FIG. 7: (Top) Phonon DOS of FeSi and $Fe_4Si_3Al$ computed with DFT, at the theoretical lattice constants ($a = 4.4492\mathring{A}$ and $a = 4.4839\mathring{A}$), respectively. (Bottom) Phonon dispersions of FeSi and $Fe_4Si_3Al_1$ computed with DFT, as above. Red dashed lines: FeSi. Solid black lines: $Fe_4Si_3Al_1$.

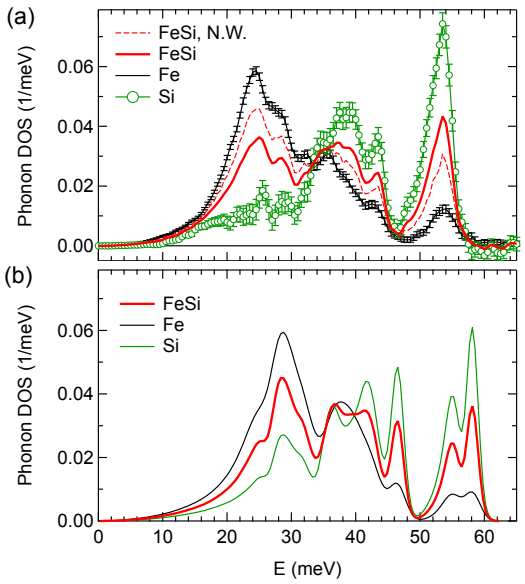


FIG. 8: (a) Total and partial phonon DOS of FeSi, obtained from NRIXS and INS measurements at $T = 300\,\mathrm{K}$. The curve labeled "FeSi, N.W." is the neutron-weighted phonon DOS obtained from INS, while "FeSi" is corrected for the effect of neutron-weighting. (b) Total and partial phonon DOS computed from first principles, at the DFT equilibrium lattice constant ($a = 4.4492\mathring{A}$), and convoluted with the experimental energy resolution.

shown in Fig. 7. A significant softening also occurs upon substitution of Si by Al, which is combined consequence of increased volume and increased screening by extra carriers. The calculated total and partial DOS are compared with the INS and NRIXS data in Fig. 8. As can be seen on this figure, both the total and partial phonon DOSs for FeSi are in good agreement with our measurements. All the peaks are reproduced, with closely matching energies and intensities. The calculated spectra are shifted to higher energy because the theoretical lattice parameter underestimates the experimental value at 300 K.

The average Grüneisen parameter, $\bar{\gamma} = -d\ln\langle E\rangle/d\ln V$, was computed for the total DOS, as well as the partial DOSes, by computing the phonons at several different lattice parameters. Our results are $\bar{\gamma}_{\mathrm{tot}}(\mathrm{FeSi}) = 1.61$, $\bar{\gamma}_{\mathrm{Fe}}(\mathrm{FeSi}) = 1.60$, and $\bar{\gamma}_{\mathrm{Si}}(\mathrm{FeSi}) = 1.62$, indicating little mode-dependence of the Grüneisen parameter. The Grüneisen parameter was also calculated for $Fe_4Si_3Al_1$, and a very similar value was obtained: $\bar{\gamma}_{\mathrm{tot}}(Fe_4Si_3Al_1) = 1.66$. Thus, in DFT calculations that do not include the effect of thermal disorder (with static ions at equilibrium positions), the amount of anharmonicity is the same in FeSi and FeSi(Al). We have shown in[23] that this conclusion is changed significantly in FeSi when the ions sample more realistic, displaced positions corresponding to finite temperatures. A similar conclusion is reached in the discussion below by comparing the dependences of phonons on temperature and pressure.

## VI. DISCUSSION

Having both the $T$ and $P$ dependence of the phonon energies $E = \hbar\omega = \hbar\omega(V,T)$ (where $V = V(P,T)$), we can estimate the intrinsic temperature dependence, $\partial E/\partial T)_V$ using the relation:

$$\frac{\partial \ln\langle E\rangle}{\partial T}\Big)_P = -3\alpha\, B\, \frac{\partial \ln\langle E\rangle}{\partial P}\Big)_T + \frac{\partial \ln\langle E\rangle}{\partial T}\Big)_V ,$$

where $\alpha$ is the linear coefficient of thermal expansion, and $B$ is the bulk modulus. For a conventional harmonic system, or even a quasi-harmonic one in which $E = E(V)$, the last term is zero, as the energy levels are equidistant and thus the vibration frequency is independent of the occupation number. A non-zero intrinsic $T$ dependence can arise from anharmonicity in the interatomic potential (departure from quadratic potential), or from a $T$-dependent harmonic potential, corresponding to $T$-dependent force-constants. We have previously shown that frozen-phonon potentials are mostly harmonic in FeSi, but that the metallization leads to a strong intrinsic $T$ dependence[23].

We evaluate the different terms above for FeSi near ambient conditions, using $\alpha = 1.4\times10^{-5}\,\mathrm{K}^{-1}$ from[47] and $B = 185\,\mathrm{GPa}$ from[8]. Assuming that the $P$ dependence of $\langle E\rangle$ and $\langle E_{\mathrm{Fe}}\rangle$ measured with NRIXS are similar (a safe assumption according to the volume dependence of the partial and total phonon DOS in our DFT calculations), we find that the first term on the right is $-8.3\times10^{-5}\,\mathrm{K}^{-1}$. On the other hand, from our INS data for FeSi in Fig. 2-a, we obtain $\partial\ln\langle E\rangle/\partial T)_P = -16.5\times10^{-5}\,\mathrm{K}^{-1}$. This yields $\partial\ln\langle E\rangle/\partial T)_V = -8.2\times10^{-5}\,\mathrm{K}^{-1}$. Thus, in FeSi, the intrinsic temperature dependence of interatomic force-constants accounts for about half of the observed rate of temperature softening in FeSi around 300 K –a large amount at this modest temperature–, which is qualitatively consistent with the behavior of the thermal expansion discussed above. For comparison, our INS data for $FeSi_{0.9}Al_{0.1}$ give $\partial\ln\langle E\rangle/\partial T)_P = -7.6\times10^{-5}\,\mathrm{K}^{-1}$ at 300 K, thus indicating a much better agreement with the quasi-harmonic model.

These results indicate that the metallization of FeSi induces a large change in the interatomic force-constants and potential energy surface felt by the ions, which leads to both a strong decrease of the average phonon energy, and a large increase in thermal expansivity. We note that the change in the potential energy surface does not affect all phonon modes equally, as can be seen in the spread of values in Fig. 2-b, although all the phonons we measured have a stronger-than-normal softening.

Previous results showed that the narrow band gap of FeSi makes this material sensitive to thermal disorder as well as alloying[19,23], and that the metallization induced by increased temperature or alloying leads to a significant softening of the phonons. We have shown here that

the introduction of either holes (Al doping) or electrons (Co doping) leads to a softening of the phonons at low-temperate by screening the interatomic force-constants, and also recovers a normal temperature dependence of the phonons, as the doped compounds are metallic at all temperatures.

A similar adiabatic electron-phonon coupling has been shown to induce an anomalous stiffening of phonons with increasing temperature in superconducting vanadium-based BCC alloys and A15 compounds[33,34]. In that case, the anomaly was shown to arise from the presence of a sharp peak in the electronic density of states (DOS) at the Fermi level. With increasing $T$, the peak at $E_{\mathrm{F}}$ gets broadened by thermal disorder, leading to a suppression in $N(E_{\mathrm{F}})$. While originating with the same mechanism, the adiabatic electron-phonon coupling in these V superconductors and in FeSi naturally gives rise to reverse anomalies in the temperature dependence of phonon frequencies[23,33,34]. Thus, both types of systems illustrate the importance of the coupling between phonons and electron states when the band structure exhibits sharp features near the Fermi level, and the importance of including thermal atomic disorder in finite-temperature electronic structure calculations.

## VII. CONCLUSIONS

The phonon spectra of FeSi and $\mathrm{FeSi}_{1-x}\mathrm{Al}_x$ were measured as a function of temperature and as a function of pressure with a combination of INS and NRIXS techniques, and compared to first-principles calculations. While FeSi displays an anomalously strong phonon softening with increasing temperature, $\mathrm{FeSi}_{0.9}\mathrm{Al}_{0.1}$ follows the regular quasi-harmonic behavior, similar to CoSi. This establishes that the metallization of the system by doping carriers has the same effect on the phonons as the temperature-induced filling of the gap by thermal disorder, previously reported by the authors and others[19,23]. In addition, the pressure dependence of the phonons at room temperature in FeSi is also conventional, and well reproduced by DFT calculations as a function of volume. By combining the results as a function of pressure and temperature, we showed that the metallization of FeSi leads to a softening of the potential energy surface for ions, which accounts for a large portion of the temperature dependence of phonon energies.

## VIII. ACKNOWLEDGEMENTS

O.D. and B.S. acknowledge funding from the US DOE, Office of Basic Energy Sciences, Materials Sciences and Engineering Division. J.M. was supported by the US DOE, Office of Basic Energy Sciences, as part of an Energy Frontier Research Center, DOE Grant DE-SC0001299. The phonon modeling work was sponsored by the Laboratory Directed Research and Development Program of Oak Ridge National Laboratory, managed by UT-Battelle, LLC, for the U. S. Department of Energy.. The Research at Oak Ridge National Laboratorys Spallation Neutron Source was sponsored by the Scientific User Facilities Division, Office of Basic Energy Sciences, US Department of Energy (DOE). Use of the HPCAT facility was supported by DOE-BES, DOE-NNSA (CDAC), NSF, DOD TACOM, and the W.M. Keck Foundation. Use of the APS was supported by DOE-BES, under Contract No. DE-AC02-06CH11357.

[1] L. Pauling and A. M. Soldate, Acta Cryst. **1**, 212 (1948).
[2] D. P. Dobson, L. Vocadlo and I.G. Wood, American Mineralogist 87, 784 (2002).
[3] J. Kunes and V.I. Anisimov, Phys. Rev. B **78**, 033109 (2008).
[4] M. Arita et al., Phys. Rev. B **77**, 205117 (2008).
[5] M. Klein, D. Zur, D. Menzel, J. Schoenes, K. Doll, J. Röder and F. Reinert, Phys. Rev. Letters **101**, 046406 (2008).
[6] N. Manyala, J.F. DiTusa, G. Aeppli and A.P. Ramirez, Nature **454**, 976 (2008).
[7] E. Knittle and Q. Williams, Geophys. Res. Letters **22**, 445 (1995).
[8] J.F. Lin, A.J. Campbell, D.L. Heinz and Guoyin Shen, Journal of Geophysical Research 108, 2045 (2003).
[9] R. Caracas and R. Wentzcovitch, Geophysical Research Letters 31, L20603 (2004).
[10] J. F. DiTusa, K. Friemelt, E. Bucher, G. Aeppli, and A. P. Ramirez, Phys. Rev. Letters **78**, 2831 (1997).
[11] J. F. DiTusa, K. Friemelt, E. Bucher, G. Aeppli, A. P. Ramirez , Phys. Rev. B **58**, 10288 (1998).
[12] V. Jaccarino, G. K. Wertheim, J. H. Wernick, L. R. Walker, and Sigurds Arajs, Phys. Rev. **160**, 476 (1967)
[13] L.F. Mattheiss and D.R. Hamann, Phys. Rev. B **47**, 13114 (1993).
[14] C. Fu, M.P.C.M. Krijn and S. Doniach, Phys. Rev. B **49**, 2219 (1994).
[15] B.C. Sales, E.C. Jones, B.C. Chakoumakos, J.A. Fernandez-Baca, H.E. Harmon, J.W. Sharp, and E.H. Volckmann, Phys. Rev. B **50**, 8207 (1994)
[16] D. Mandrus, J.L. Sarrao, A. Migliori, J.D. Thompson and Z. Fisk, Phys Rev. B **51**, 4763 (1995).
[17] R. P. Krentsis, G. I. Kalishevich, P. V. Geld, and L. P. Andreeva, Izv. Vyssh. Vchebon. Zaved. Fiz. **1**, 153 (1972) [Sov. Phys. **15**, 193 (1972)].
[18] V. I. Anisimov, S. Y. Ezhov, I. S. Elfimov, I. V. Solovyev, and T. M. Rice, Phys. Rev. Letters **76**, 1735 (1996).
[19] T. Jarlborg, Physics Letters A **236**, 143 (1997).
[20] T. Jarlborg, Phys. Rev B **59** 15002 (1999).
[21] T. Jarlborg, J. Magn. Magn. Mater. **283**, 238246 (2004).
[22] T. Jarlborg, Phys. Rev. B 76, 205105 (2007).
[23] O. Delaire, K. Marty , M. B. Stone, P. R. C. Kent, M. S. Lucas, D. L. Abernathy, D. Mandrus, B. C. , , Proc. Natl. Acad. Sci. USA **108**, 4725 (2011).
[24] B. C. Sales, O. Delaire, M. A. McGuire, and A. F. May, Phys. Rev. B **83**, 125209 (2011).
[25] J. M. Tomczak, K. Haule, and G. Kotliar, Proc. Natl. Acad. Sci. USA **109** 3243-3246 (2012).
[26] D. Zur, D. Menzel, I. Jursic, J. Schoenes, L. Patthey, M. Neef, K. Doll, and G. Zwicknagl, Phys. Rev. B **75**, 165103 (2007).
[27] D. Menzel, P. Popovich, N. N. Kovaleva, J. Schoenes, K. Doll, and A. V. Boris, Phys. Rev. B **79**, 165111 (2009).
[28] K. Ishizaka, T. Kiss, T. Shimojima, T. Yokoya, T. Togashi, S. Watanabe, C. Q. Zhang, C. T. Chen, Y. Onose, Y. Tokura, and S. Shin, Phys. Rev. B **72** 233202 (2005).
[29] L. Degiorgi, M. B. Hunt, H. R. Ott, M. Dressel, B. J. Feenstra, G. Grner, Z. Fisk and P. Canfield, Europhys. Lett. **28**, 341 (1994).
[30] A. Damascelli, K. Schulte, D. van der Marel, and A. A. Menovsky, Phys. Rev. B **55**, R4863 (1997).
[31] A.-M. Racu, D. Menzel, J. Schoenes, and K. Doll, Phys. Rev. B **76**, 115103 (2007).
[32] H. Kim and M. Kaviany, Phys. Rev. B **86**, 045213 (2012).
[33] O. Delaire, M. S. Lucas, J. A. Muñoz, M. Kresch, and B. Fultz, Phys. Rev. Letters **101**, 105504 (2008).
[34] O. Delaire, M. Kresch, J. A. Muñoz, M. S. Lucas, J. Y. Y. Lin, and B. Fultz, Phys. Rev. B **77**, 214112 (2008).
[35] O. Delaire, A. F. May, M. A. McGuire, W. D. Porter, M. S. Lucas, M. B. Stone, D. L. Abernathy, V.A. Ravi, S. A. Firdosy and G. J. Snyder, Phys. Rev. B **80**, 184302 (2009)
[36] C. Candolfi, B. Lenoir, and A. Dauscher, M. M. Koza, M. de Boissieu, M. Sternik and K. Parlinski, Phys. Rev. B **84**, 224306 (2011).
[37] Xiaoya Shi, Yanzhong Pei, G. Jeffrey Snyder, and Lidong Chen, Energy Environ. Sci. **4**, 40864095 (2011).
[38] B. T. Fultz, Progress in Materials Science, **55**, 247 (2010).
[39] Y. Onose, N. Takeshita, C. Terakura, H. Takagi, and Y. Tokura, Phys. Rev. B **72**, 224431 (2005).
[40] S. V. Grigoriev, V. A. Dyadkin, D. Menzel, J. Schoenes, Yu. O. Chetverikov, A. I. Okorokov, H. Eckerlebe, and S. V. Maleyev, Pys. Rev. B **76**, 224424 (2007).
[41] X. Z. Yu, Y. Onose, N. Kanazawa, J. H. Park, J. H. Han, Y. Matsui, N. Nagaosa, and Y. Tokura, Nature **465**, 901 (2010).
[42] D. L. Abernathy, M. B. Stone, M. J. Loguillo, M. S. Lucas, O. Delaire, X. Tang, J.Y.Y. Lin, and B. Fultz, Rev. Sci. Instrum. **83**, 15114 (2012).
[43] http://www.mantidproject.org
[44] M. Kresch, O. Delaire, R. Stevens, J.Y.Y. Lin and B. Fultz, Phys. Rev. B, **75**, 104301 (2007).
[45] J. L. Sarrao, D. Mandrus, A. Migliori, Z. Fisk, E. Bucher, Physica B **199-200**, 478-479 (1994).
[46] A. E. Petrova, V. N. Krasnorussky, A. A. Shikov, W. M. Yuhasz, T. A. Lograsso, J. C. Lashley, and S. M. Stishov, Phys. Rev. B **82**, 155124 (2010).
[47] L. Vočadlo, K.S. Knight, G.D. Price and I.G. Wood, Phys. Chem. Minerals **29**, 132 (2002).
[48] G. Grimvall, *Thermophysical Properties of Materials* (North Holland, Amsterdam, 1999).
[49] E. E. Alp, W. Sturhahn, T.S. Toellner, J. Zhao, M. Hu, and D.E. Brown, Hyperfine Interactions **144/145**, 3 (2002).
[50] W. Sturhahn, T.S. Toellner, E.E. Alp, X. Zhang, M. Ando, Y. Yoda, S. Kikuta, M. Seto, C.W. Kimball, and B. Dabrowski, Phys. Rev. Letters **74**, 3832 (1995).
[51] W. Sturhahn, Hyper. Inter. **125**, 149 (2000).
[52] G.J. Piermarini, S. Block, J.D. Barnett, R.A. Forman, Journal of Applied Physics **46(6)**, 2774 (1975)
[53] G. Kresse and J. Furthmüller, Phys. Rev. B **54**, 11169 (1996).
[54] P.E. Blöchl, Phys. Rev. B **50**, 17953 (1994).
[55] G. Kresse and D. Joubert, Phys. Rev. B **59**, 1758 (1999).
[56] J.P. Perdew, K. Burke and M. Ernzerhof, Phys. Rev. Lett. **77**, 3865 (1996).